Journal of Power Sources 190 (2009) 513–524

Contents lists available at ScienceDirect

Journal of Power Sources

journal homepage: www.elsevier.com/locate/jpowsour

Photocatalytic H_2 production from water splitting under visible light irradiation using Eosin Y-sensitized mesoporous-assembled Pt/TiO_2 nanocrystal photocatalyst

Thammanoon Sreethawong[a,b,*], Chompoonuch Junbua[a], Sumaeth Chavadej[a,b]

[a] The Petroleum and Petrochemical College, Chulalongkorn University, Soi Chula 12, Phyathai Road, Pathumwan, Bangkok 10330, Thailand
[b] Center for Petroleum, Petrochemicals, and Advanced Materials, Chulalongkorn University, Bangkok 10330, Thailand

ARTICLE INFO

Article history:
Received 10 October 2008
Received in revised form 9 December 2008
Accepted 4 January 2009
Available online 30 January 2009

Keywords:
Hydrogen production
Sensitization
Titania
Mesoporous assembly
Visible light
Photocatalytic water splitting

ABSTRACT

Sensitized photocatalytic production of hydrogen from water splitting is investigated under visible light irradiation over mesoporous-assembled titanium dioxide (TiO_2) nanocrystal photocatalysts, without and with Pt loading. The photocatalysts are synthesized by a sol–gel process with the aid of a structure-directing surfactant and are characterized by N_2 adsorption–desorption analysis, X-ray diffraction, UV–vis spectroscopy, scanning electron microscopy, transmission electron microscopy and energy-dispersive X-ray analysis. The dependence of hydrogen production on the type of TiO_2 photocatalyst (synthesized mesoporous-assembled and commercial non-mesoporous-assembled TiO_2 without and with Pt loading), the calcination temperature of the synthesized photocatalyst, the sensitizer (Eosin Y) concentration, the electron donor (diethanolamine) concentration, the photocatalyst dosage and the initial solution pH is systematically studied. The results show that in the presence of the Eosin Y sensitizer, the Pt-loaded mesoporous-assembled TiO_2 synthesized by a single-step sol–gel process and calcined at 500 °C exhibits the highest photocatalytic activity for hydrogen production from a 30 vol.% diethanolamine aqueous solution with dissolved 2 mM Eosin Y. Moreover, the optimum photocatalyst dosage and initial solution pH for the maximum photocatalytic activity for hydrogen production are 3.33 g dm^{-3} and 11.5, respectively.

1. Introduction

At present, all conventionally available energy resources, especially coal and fossil fuels, are being greatly and irreversibly consumed because they are in huge demand world-wide. Even though the price of these resources fluctuates, their use is continuously expanding for many applications, some without concern for the environmental impact. A vast amount of carbon dioxide (CO_2) is produced from the aforementioned uses, and its uncontrolled release into the atmosphere is resulting in global warming [1]. Additionally, these conventional fuels will reportedly be in short supply in the near future. Therefore, many attempts have focused on hydrogen as an alternative and renewable energy source for future demands [2–4].

Hydrogen is now being recognized as an ideal energy source for the future due to its versatile application, environmentally friendly properties, and several other acceptable standpoints. In particular, no harmful products (e.g., CO_2, smog and particulates) are generated or emitted to the environment from the combustion of hydrogen, unlike the combustion of conventional fuel resources. The hydrogen can be employed for various technologies, such as in non-polluting vehicles and aircraft, domestic heating, and power generation via fuel cells [5,6]. Hence, safe, pollution-free and sustainable hydrogen production technologies need to be extensively investigated and developed to meet future energy requirements.

Photocatalytic water splitting is a chemical reaction for producing hydrogen by using two major renewable energy resources, namely, water and solar energy. Water, as the feedstock for the reaction, is clean, inexpensive and available in a virtually inexhaustible reserve, whereas solar energy is also infinitely available, non-polluting and appropriate for the endothermic water splitting reaction. The water splitting reaction can be achieved without generating any polluting by-products [7,8]. The use of a semiconductor photocatalyst is a promising technique because the photocatalyst is in a solid phase form and is secure for use, resistant to deactivation, chemically stable and environmentally friendly. Among the various types of widely-investigated semiconductor material, titanium dioxide (TiO_2) has been considered the most active photocatalyst because of its comparatively high photocatalytic efficiency [9,10].

* Corresponding author at: The Petroleum and Petrochemical College, Chulalongkorn University, Soi Chula 12, Phyathai Road, Pathumwan, Bangkok 10330, Thailand. Tel.: +66 2 218 4144; fax: +66 2 215 4459.
E-mail address: thammanoon.s@chula.ac.th (T. Sreethawong).

0378-7753/$ – see front matter © 2009 Elsevier B.V. All rights reserved.
doi:10.1016/j.jpowsour.2009.01.054

Its large band gap energy (3.2 eV for anatase TiO_2) limits its use for photocatalytic water splitting under visible light irradiation, with wavelengths between 400 and 700 nm, which occupies a large portion of the solar spectrum (approximately 42%) that hits the earth's surface; it can only be utilized under ultraviolet irradiation (approximately 8% of the incoming solar energy). To realize photocatalytic water splitting over TiO_2 under visible light irradiation, it is necessary to modify the TiO_2 chemical structure to make it able to respond to visible light.

In order to modify the photocatalytic ability of these TiO_2 photocatalysts so as to use visible light, several available techniques need to be taken into consideration, namely, metal ion doping, anion doping, the mixing of two semiconductors having large and small band gap energies, and sensitization by visible light-absorbing sensitizers (dyes, in most cases) [11,12]. The sensitization of semiconductor photocatalysts is a very promising approach because it not only enables the absorption of visible light, but also the photocatalyst system does not suffer detrimental photodecomposition. The visible light initially excites the sensitizer molecules adsorbed on the TiO_2 surface, and the electrons are then injected directly into the conduction band of the TiO_2, or indirectly through the loaded metal. The conduction band and the loaded metal particles behave either as a mediator for transferring electrons from the excited sensitizer or as a substrate for accepting electrons for the photocatalytic reaction. The valence band is not usually involved in the sensitization process [11,12]. After losing electrons via the charge-transfer process, electron donors (sacrificial agents), such as diethanolamine (DEA), triethanolamine (TEA) and ethylenediaminetetraacetic acid (EDTA), are usually added to the reaction solution to regenerate the electron-deficient sensitizer and thereby sustain the photoreaction cycle [12–14]. The sensitization of TiO_2 by various compounds, such as Eosin Y (E.Y.), $Ru(bpy)_3^{2+}$, $[Ru(dcpy)_2(dpq)]^{2+}$, merocyanine and coumarin, has been examined [14–19].

Eosin Y-sensitized systems, employing not only TiO_2 but also other active photocatalysts, have been extensively studied owing to the markedly enhanced photocatalytic activity for hydrogen production from water splitting. Abe et al. [16] studied the Eosin Y sensitization of four commercial TiO_2 powders without and with platinum (Pt) loading in the presence of a silane-coupling agent and TEA for photocatalytic hydrogen production. Several studies have been undertaken on the Eosin Y sensitization of noble metal-loaded TiO_2 (noble metal = Pt, Ru and Rh) [16], Pt-loaded $Na_2Ti_2O_4(OH)_2$ nanotubes [20], Pt-loaded silica gel [21], Pt-loaded nitrogen-doped TiO_2 (the TiO_2 was prepared by the hydrolysis of $Ti(SO_4)_2$) [22] and Pt-loaded TS-1 zeolite [23] for photocatalytic hydrogen production. There is, however, no report of the use of a mesoporous-assembled TiO_2 nanocrystal photocatalyst for such a purpose. Moreover, since it is clearly stated in the literature cited above that Pt loading can enhance photocatalytic hydrogen production from a sensitization system, the use of a Pt-loaded mesoporous-assembled TiO_2 nanocrystal photocatalyst synthesized by a single-step sol–gel (SSSG) process for this photocatalytic reaction (which has not been reported elsewhere) is also very interesting.

This work, therefore, focuses on photocatalytic hydrogen production via a water splitting reaction by using a mesoporous-assembled TiO_2 nanocrystal photocatalyst suspension with a sensitizer (Eosin Y) under visible light irradiation in the presence of an electron donor (DEA). By following previous reports of the synthesis of mesoporous-assembled TiO_2 photocatalysts without and with Pt loading via a sol–gel process, with the aid of a structure-directing surfactant [24,25], the synthesized photocatalysts are further used for sensitized photocatalytic activity testing, compared with many commercially available non-mesoporous-assembled TiO_2 photocatalysts. Because the mesoporous-assembled TiO_2 nanocrystal possesses a large surface area and pore volume for reactant accessibility, and uniform pore size distribution, it is very desirable to apply this material, for the first time, to sensitized photocatalytic hydrogen production. The effects of preparation conditions and Pt loading on the physical properties of the photocatalysts and on the photocatalytic hydrogen production activity are investigated. Several reaction parameters – such as Eosin Y concentration, DEA concentration, photocatalyst dosage and initial solution pH – are also systematically studied.

2. Experimental

2.1. Materials

All chemical reagents used for photocatalyst synthesis and photocatalytic activity testing were of analytical grade and were used without further purification. Tetraisopropyl orthotitanate [TIPT, $Ti(OCH(CH_3)_2)_4$), Merck], laurylamine hydrochloride [LAHC, $CH_3(CH_2)_{11}NH_2{\cdot}HCl$), Merck], acetylacetone (ACA, $CH_3COCH_2COCH_3$, Rasayan), hydrogen hexachloroplatinate (IV) hexahydrate ($H_2PtCl_6{\cdot}6H_2O$, Aldrich), diethanolamine [$(HOCH_2CH_2)_2NH$, Lab Scan] and Eosin Y ($C_{20}H_6Br_4Na_2O_5$, Aldrich) were used. The TIPT was used as a titanium precursor for synthesizing the TiO_2 photocatalyst. The LAHC was used as a structure-directing surfactant; it behaves as both a mesopore-forming and a gelation-assisting agent. The ACA served as a modifying agent, which was used to moderate the hydrolysis and condensation steps. The $H_2PtCl_6{\cdot}6H_2O$ was used as a precursor of the Pt co-catalyst acting as hydrogen production active sites. Commercially available TiO_2 powders, namely P-25 (J.J. Degussa Hüls Co. Ltd.), ST-01 (Ishihara Sangyo Co. Ltd.), JRC-01 (Ishihara Sangyo Co. Ltd.) and JRC-03 (Ishihara Sangyo Co. Ltd.), were selected for comparative studies of photocatalytic hydrogen production with synthesized mesoporous-assembled TiO_2 nanocrystal photocatalysts.

2.2. Photocatalyst synthesis procedure

A mesoporous-assembled TiO_2 nanocrystal photocatalyst was synthesized via a sol–gel process with the aid of a structure-directing surfactant in a system consisting of LAHC and ACA-modified TIPT [24]. First, a specified amount of ACA was introduced into the TIPT with a molar ratio of unity. Then, the solution was continuously stirred at room temperature until a homogeneous state was achieved. This caused a change in the coordination number of the Ti atoms from 4 to 5 (clearly seen from a change in the solution colour from colourless to yellow). The obtained ACA-modified TIPT was less active to moisture in the atmosphere than the unmodified TIPT. Afterwards, a 0.1 M LAHC aqueous solution, with a pH of 4.2, was added to the ACA-modified TIPT solution, in which the molar ratio of TIPT to LAHC was adjusted to a value of 4 in order to control the porosity of the TiO_2 photocatalyst. The mixed solution was continuously stirred at 40 °C for 8 h to obtain a transparent yellow sol. For the case of Pt-loaded TiO_2, a required amount of hydrogen hexachloroplatinate (IV) hydrate for the desired Pt loading of 0.6 wt.% (optimally providing the highest photocatalytic activity for the Pt-loaded mesoporous-assembled TiO_2 photocatalyst synthesized by a SSSG process) was incorporated into the aged transparent sol solution [25]. The resultant mixture was further aged at 40 °C for 2 h to acquire a homogeneous solution. The gel was then formed by placing the sol-containing solution in an oven at 80 °C for a week for complete gel formation. Afterwards, the gel was dried at 80 °C overnight. Finally, the dried gel was calcined at 500–700 °C for 4 h to remove the LAHC template, and subsequently the desired photocatalyst was achieved.

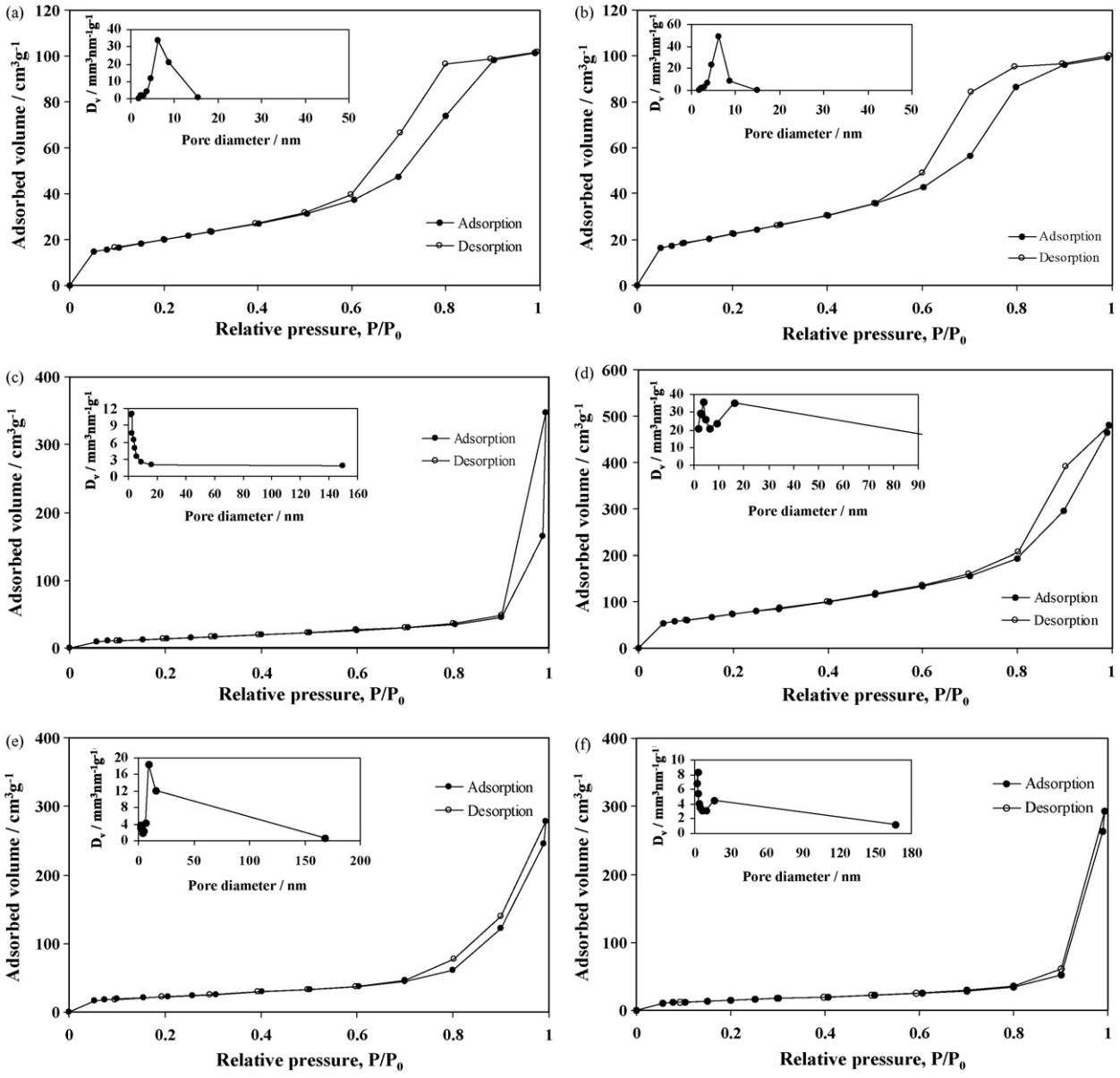

Fig. 1. N_2 adsorption–desorption isotherms of: (a) synthesized mesoporous-assembled TiO_2 calcined at 500 °C for 4 h; (b) 0.6 wt.% Pt-loaded mesoporous-assembled TiO_2 calcined at 500 °C for 4 h; (c) commercial P-25 TiO_2; (d) commercial ST-01 TiO_2; (e) commercial JRC-01 TiO_2; (f) commercial JRC-03 TiO_2 (inset: pore size distributions).

2.3. Photocatalyst characterization techniques

A surface area analyzer (Quantachrome/Autosorb 1) was used to obtain the adsorption–desorption isotherms of all the investigated photocatalysts at a liquid nitrogen temperature (−196 °C). The Brunauer–Emmett–Teller (BET) approach using adsorption data over a relative pressure that ranged from 0.05 to 0.35 was employed to determine the specific surface area of all the studied photocatalyst samples. The Barrett–Joyner–Halenda (BJH) approach was used for calculating the mean pore size and pore size distribution. X-ray diffraction (XRD) was used to identify the structure and the composition of the photocatalysts. A Rigaku/Rint2200 HV diffractometer, equipped with a Ni-filtered CuKα radiation source (λ = 1.542 Å) in continuous scanning mode at the rate of 5° min^{-1} operating at 40 kV and 30 mA, was used to obtain the XRD patterns. The sample was degassed at 150 °C for 2 h to remove the physisorbed gases prior to analysis. A Shimadzu UV-2550 UV–vis spectrophotometer was used to record the absorbance spectra of the photocatalysts, with $BaSO_4$ as the reference, as well as that of the Eosin Y solution, by operating at room temperature under a scanning wavelength of 200–900 nm. The surface morphology of the photocatalyst samples was observed by means of a scanning electron microscope (SEM, JEOL 5200-2AE) and a transmission electron microscope (TEM, JEOL 2000 CX) operating at 15 and 200 kV, respectively. Elemental mapping over the desired region of the photocatalyst was obtained by using an energy-dispersive X-ray analyzer (EDX) attached to both the SEM and TEM. The selected-area electron diffraction (SAED) mode attached to the TEM was also used to confirm the photocatalyst structure.

2.4. Photocatalytic hydrogen production experiments

Photocatalytic activity testing was performed in a closed-gas Pyrex glass reactor at room temperature. In a typical run, a specified amount (0.2 g) of each of the prepared photocatalysts – namely synthesized mesoporous-assembled TiO_2, commercial TiO_2 (P-25, ST-01, JRC-01 and JRC-03) and 0.6 wt.% Pt-loaded mesoporous-assembled TiO_2 – was suspended in 150 cm^3 of an aqueous

Table 1
Summary of N_2 adsorption–desorption results for synthesized mesoporous-assembled TiO_2, 0.6 wt.% Pt-loaded mesoporous-assembled TiO_2, P-25 TiO_2, ST-01 TiO_2, JRC-01 TiO_2 and JRC-03 TiO_2.

Photocatalyst	Calcination temperature (°C)	Calcination time (h)	BET surface area ($m^2\ g^{-1}$)	Mean pore diameter (nm)	Total pore volume ($cm^3\ g^{-1}$)
Mesoporous-assembled TiO_2	500	4	84.13	6.16	0.157
	600	4	22.67	8.82	0.053
	700	4	8.74	–[a]	–[a]
0.6 wt.% Pt-loaded mesoporous-assembled TiO_2	500	4	94.98	6.18	0.153
P-25 TiO_2	–	–	65.03	–[a]	–[a]
ST-01 TiO_2	–	–	289.5	–[a]	–[a]
JRC-01 TiO_2	–	–	84.07	–[a]	–[a]
JRC-03 TiO_2	–	–	54.98	–[a]	–[a]

[a] N_2 adsorption–desorption isotherm corresponds to IUPAC type II pattern.

Table 2
Summary of XRD analysis of synthesized mesoporous-assembled TiO_2, 0.6 wt.% Pt-loaded mesoporous-assembled TiO_2 and commercial TiO_2.

Photocatalyst	Calcination temperature (°C)	Calcination time (h)	Phase from XRD pattern	Rutile ratio (W_R)	Crystallite size (nm)	
					Anatase (1 0 1)	Rutile (1 1 0)
Mesoporous-assembled TiO_2	500	4	Anatase	–	13.64	–
	600	4	Anatase + Rutile	0.05	25.75	46.26
	700	4	Anatase + Rutile	0.79	38.75	53.96
0.6 wt.% Pt-loaded mesoporous-assembled TiO_2	500	4	Anatase	–	12.21	–
P-25 TiO_2	–	–	Anatase + Rutile	0.26	22.01	28.90
ST-01 TiO_2	–	–	Anatase	–	8.33	–
JRC-01 TiO_2	–	–	Anatase	–	15.35	–
JRC-03 TiO_2	–	–	Rutile	1.00	–	17.11

diethanolamine solution containing the dissolved Eosin Y sensitizer by using a magnetic stirrer. Prior to the reaction, the mixture was purged with Ar gas for 45 min in a dark environment to establish adsorption equilibrium (as well as to remove the air from the reactor). The reaction was commenced by exposing the mixture to visible light irradiation from a 300 W Xe arc lamp (Type KXL-300/WACOM Electric, light intensity = 2.6 mW cm^{-2}), emitting light with wavelengths longer than 400 nm using a UV cut-off filter (B-48S/ATG). The gaseous H_2 inside the reactor was periodically withdrawn by a gas-tight syringe and analyzed with a gas chromatograph (GC, PerkinElmer/ARNEL, HayeSep D, Argon gas) equipped with a thermal conductivity detector (TCD).

3. Results and discussion

3.1. Photocatalyst characterization results

3.1.1. N_2 adsorption–desorption results

N_2 adsorption–desorption analysis was used to verify the mesoporosity of the studied photocatalysts since the isotherm shape reveals the characteristics of a powder structure, which consists of an assembly of numerous particles with large open packing. The adsorption–desorption isotherms of the unloaded mesoporous-assembled TiO_2 and the 0.6 wt.% Pt-loaded mesoporous-assembled TiO_2 nanocrystals prepared by the SSSG process calcined at 500 °C are shown in Fig. 1(a) and (b), respectively. The isotherms reveal the typical IUPAC type IV pattern with the H2 hysteresis loop, which is characteristic of a mesoporous-assembled material (mesopore size between 2 and 50 nm) according to the classification of IUPAC [26]. A sharp increase in the adsorption volume of N_2 was clearly observed, located in the P/P_0 range of 0.5–0.9. This sharp increase can be attributed to the capillary condensation of N_2 inside the mesopores, indicating good homogeneity of the sample and a fairly small pore size, since the P/P_0 position of the inflection point is directly related to the pore dimension. The insets of Fig. 1(a) and (b) show the pore size distribution curves calculated from the desorption branch of the isotherms by the BJH method. It is clear that the samples possess monomodal and very narrow pore size distribution, which is also a demonstration of the good quality of the samples. Fig. 1(b) reveals that the Pt loading does not greatly affect the structure of the synthesized mesoporous-assembled TiO_2.

With the commercial P-25 TiO_2, ST-01 TiO_2, JRC-01 TiO_2 and JRC-03 TiO_2 photocatalysts, the N_2 adsorption–desorption isotherms for all of them correspond to the IUPAC type II pattern [26], as shown in Fig. 1(c)–(f), respectively. It can be seen that all commercial TiO_2 photocatalysts possess the non-mesoporous characteristic, due to the absence of both a distinct hysteresis loop and an adsorption plateau at very high relative pressure, indicating that there is no capillary condensation of N_2 into the pores. The pore size distributions of all of the commercial TiO_2 photocatalysts, as shown in the insets of Fig. 1(c)–(f), are quite broad. These results show that the average pores of the commercial photocatalysts used are quite spacious because their pore size distributions are not only present in the mesoporous region (mesopore size between 2 and 50 nm) but also mostly exist in the macroporous region (pore diameter >50 nm).

The textural properties obtained from the N_2 adsorption–desorption isotherms (i.e., BET surface area, mean pore diameter and total pore volume) are summarized in Table 1. As clearly seen, the surface area of the unloaded mesoporous-assembled TiO_2 decreases from 83.13 to 8.74 $m^2\ g^{-1}$ with increasing calcination temperature from 500 to 700 °C. With increasing calcination temperature, the perceived loss in surface area is explained by pore coalescence due to the crystallization of the walls separating the mesopores. Moreover, the sintering and phase transformation of the anatase to the rutile phase are predictable [27]. This tendency subsequently causes an increase in the mean pore diameter and a decrease in the total pore volume of the bulk materials, as expected. However, the surface area of the 0.6 wt.% Pt-loaded TiO_2

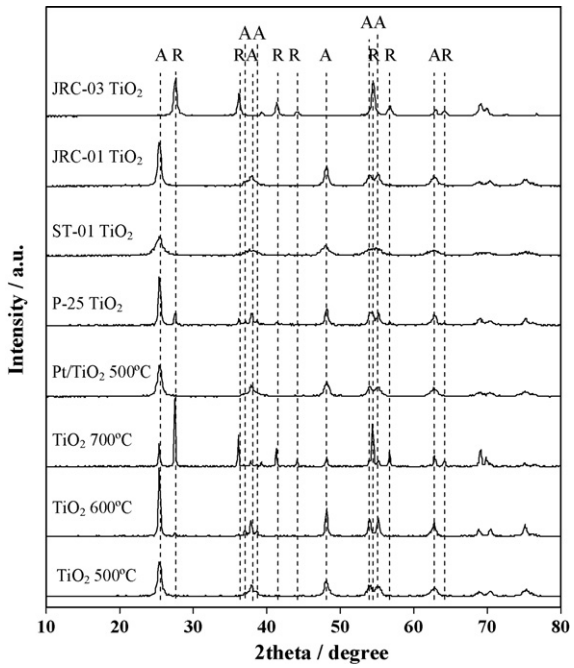

Fig. 2. XRD patterns of synthesized mesoporous-assembled TiO_2 calcined at 500–700 °C, 0.6 wt.% Pt-loaded mesoporous-assembled TiO_2 and commercial TiO_2 (A: anatase, R: rutile).

is higher than that of the unloaded TiO_2 at the calcination temperature of 500 °C. Plausibly, the loaded platinum can stabilize the TiO_2 framework to a certain degree, resulting in increased surface area due to its high dispersion on the TiO_2 surface. The N_2 adsorption–desorption isotherms of the commercial TiO_2 photocatalysts are found to correspond to the IUPAC type II pattern. The surface areas of the P-25 TiO_2 and the JRC-03 TiO_2 are lower than that of the synthesized mesoporous-assembled TiO_2 photocatalyst calcined at 500 °C for 4 h, whereas the surface area of the JRC-01 TO_2 is comparable with that of the synthesized mesoporous-assembled TiO_2. However, the surface area of the ST-01 TiO_2 is much higher than the other three commercial photocatalysts, plausibly due to its specific production procedure.

3.1.2. XRD results

The XRD patterns of all the investigated photocatalysts (mesoporous-assembled TiO_2 calcined at 500–700 °C, 0.6 wt.% Pt-loaded mesoporous-assembled TiO_2 calcined at 500 °C, and all the commercial TiO_2 photocatalysts) are shown in Fig. 2. The phase identification and crystallite size of the synthesized samples, estimated from line broadening of anatase (1 0 1) and rutile (1 1 0) diffraction peaks using Sherrer equation [28], are summarized in Table 2. The XRD pattern of the unloaded mesoporous-assembled TiO_2 calcined at 500 °C for 4 h shows the crystalline structure of the pure anatase phase. The dominant peaks at 2θ of about 25.2, 37.9, 48.3, 53.8, 62.7, 68.9 and 75.3°, which represent the indices of (1 0 1), (1 0 3), (2 0 0), (1 0 5), (2 1 3), (1 1 6) and (1 0 7) planes [29], respectively, reveal the crystalline structure of the pure anatase phase. As shown in Fig. 2, however, at the calcination temperature of 500 °C, crystallization to the anatase phase of the synthesized photocatalyst is not fully developed in comparison with that at a calcination temperature of 600 °C, at which the peak intensity of the anatase phase, especially at 2θ of 25.2°, greatly increases. A calcination temperature of 600 °C is not only determined to be the highest limit for achieving the highly crystalline pure anatase phase, but also to be the initial point of the phase transformation from the anatase to the rutile phase, since an approximately 5% rutile content

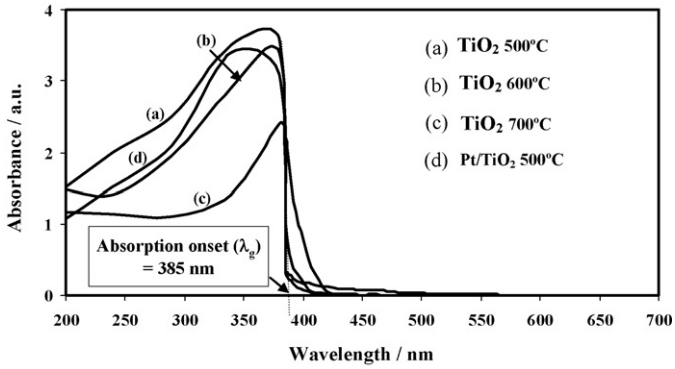

Fig. 3. UV–vis spectra of: (a)–(c) mesoporous-assembled TiO_2 calcined at 500–700 °C; (d) 0.6 wt.% Pt-loaded mesoporous-assembled TiO_2 calcined at 500 °C.

is observed. All calculated values of the rutile ratio (W_R) in terms of weight fraction are presented in Table 2. The rutile ratio is estimated from XRD intensity data by using the following relationships [30]:

$$W_R = \left[1 + \frac{0.8 I_A}{I_R}\right]^{-1} \quad (1)$$

$$W_A = 1 - W_R \quad (2)$$

where I_A and I_R represent the integrated intensities of the anatase (1 0 1) and rutile (1 1 0) diffraction peaks, respectively. At a calcination temperature of 700 °C, high phase transformation is observed and results in a combination between the anatase and the rutile phases with approximately 79% rutile content. The occurrence of the dominant peaks at 2θ of about 27.5, 36.0, 41.2, 44.1, 54.2, 56.7, 64.2 and 69.0°, which correspond to the indices of (1 1 0), (1 0 1), (1 1 1), (2 1 0), (2 1 1), (2 2 0), (3 1 0) and (3 0 1) planes [29], respectively, indicates that the rutile phase becomes the main phase in the synthesized TiO_2 photocatalyst calcined at this temperature. For the 0.6 wt.% Pt-loaded TiO_2, the dominant peak of Pt at 2θ of about 39.7° is not observed, presumably due to the combination of its low content, high degree of dispersion degree and small particle size. The results also reveal that, with increasing calcination temperature, a larger TiO_2 crystallite size is obtained. When 0.6 wt.% Pt is loaded on the mesoporous-assembled TiO_2, however, a smaller anatase crystallite size is observed, as compared with that of the unloaded TiO_2. This may confirm the role of Pt in stabilizing the TiO_2 framework from coalescence upon calcination, leading to the obtained higher surface area (Table 1). The phase identification and crystallite sizes of all the commercial TiO_2 photocatalysts are also listed in Table 2. Commercial P-25 TiO_2 shows a combined crystalline structure between anatase and rutile phases with approximately 26% rutile content, whereas commercial ST-01 TiO_2 and JRC-01 TiO_2 show only the crystalline structure of the pure anatase phase. Commercial JRC-03 TiO_2 shows only the crystalline structure of the pure rutile phase.

3.1.3. UV–vis spectra results

UV–vis spectroscopy was used to examine the light absorption ability of all the investigated photocatalysts, as well as that of the Eosin Y solution. The UV–vis spectra of the mesoporous-assembled TiO_2 calcined at 500–700 °C and the 0.6 wt.% Pt-loaded mesoporous-assembled TiO_2 are given in Fig. 3, whereas those of all the commercial photocatalysts are not presented graphically. The onset absorption wavelength and corresponding band gap energy of all the photocatalysts, as obtained from the UV–vis spectra, are summarized in Table 3. It is clearly seen that the absorption band of the synthesized mesoporous-assembled TiO_2 is in the UV light range of 200–400 nm, and the shift of the onset absorption edges

Table 3
Summary of onset absorption wavelengths and band gap energies of synthesized nanocrystalline mesoporous-assembled TiO_2 without and with Pt loading and commercial TiO_2 photocatalysts.

Photocatalyst	Calcination temperature (°C)	Calcination time (h)	Onset absorption wavelength, λ_g (nm)	Band gap energy (eV)
Mesoporous-assembled TiO_2	500	4	385	3.22
	600	4	390	3.18
	700	4	410	3.02
0.6 wt.% Pt-loaded mesoporous-assembled TiO_2	500	4	390	3.18
P-25 TiO_2	–	–	390	3.18
ST-01 TiO_2	–	–	385	3.22
JRC-01 TiO_2	–	–	380	3.26
JRC-03 TiO_2	–	–	405	3.06

toward longer wavelength with the increase in calcination temperature from 500 to 700 °C can be observed. This shift towards longer wavelength normally originates from narrowing of the band gap energy, which result in lower energy required for the excitation of electrons from the valence band to the conduction band. The band gap energy (E_g, eV) is determined by extrapolating the onset of the rising part to the *x*-axis (λ_g, nm) of the plots, as shown by the dotted line in Fig. 3 and calculated by [24]:

$$E_g = \frac{1240}{\lambda_g} \quad (3)$$

where λ_g is the wavelength (nm) of the excitation light. The band gap energy of the mesoporous-assembled TiO_2 calcined at 500 and 600 °C is approximately 3.2 eV ($\lambda_g \sim 385$ and 390 nm, respectively). The results exactly conform to the band gap energy of the anatase phase TiO_2 and, therefore, agree well with the results from the XRD analysis. For the 0.6 wt.% Pt-loaded mesoporous-assembled TiO_2, the onset absorption wavelength is approximately the same as that of the mesoporous-assembled TiO_2 calcined at 500 °C, also indicating its pure anatase phase. However, the band gap energy of the mesoporous-assembled TiO_2 calcined at 700 °C is approximately 3.0 eV ($\lambda_g \sim 410$ nm), which corresponds well to the band gap energy of the rutile phase TiO_2, as also observed from the XRD analysis. Clearly, the light absorption ability of all of the investigated TiO_2 photocatalysts is such that they can absorb only UV light of wavelengths shorter than 420 nm. Therefore, in order to confirm that the E.Y. is a visible light responding sensitizer, its UV–vis spectrum was also obtained, as shown in Fig. 4. It is clear that the E.Y. can mainly absorb visible light with a maximum absorption centred at 516 nm. This absorption feature strongly suggests that the E.Y. sensitizer can be activated by visible light for the sensitized photocatalytic system in this work.

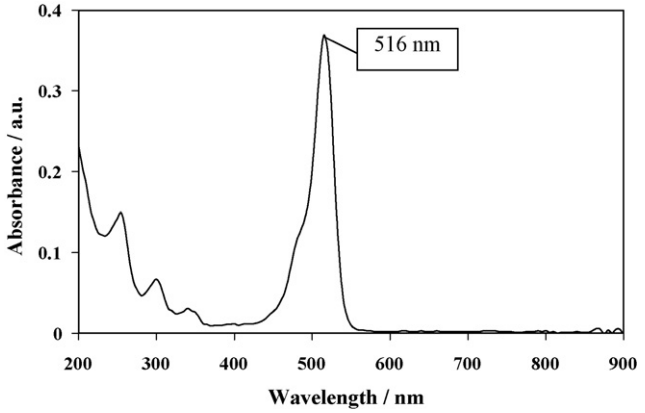

Fig. 4. UV–vis spectrum of E.Y. solution.

3.1.4. SEM–EDX results

Information concerning the surface morphologies of all the synthesized and commercial TiO_2 photocatalysts was obtained by SEM. Fig. 5 shows the SEM images of all the investigated photocatalysts. For all the synthesized TiO_2, particles with quite uniform size can be observed in the form of aggregated clusters containing many nanoparticles. This aggregation plausibly leads to the formation of the mesoporous-assembled structure. On the other hand, more segregated particles and less packed clusters can be observed for all of the commercial TiO_2 powders. The lesser degree of aggregation results in the observation, to some significant extent, of a macroporous structure. The elemental distribution of the 0.6 wt.% Pt-loaded mesoporous-assembled TiO_2 was also examined using energy-dispersive X-ray analysis by elemental area mapping of each component accompanied by its SEM image (Fig. 6). The EDX mapping show that all elements in the Pt-loaded TiO_2 are well dispersed throughout the bulk photocatalyst due to the existence of dominant dots in the elemental mapping of all the involved species (Ti, O and Pt), particularly the Pt species. This is also strong evidence for the high dispersion state of the deposited Pt particles on the TiO_2 surface.

3.1.5. TEM results

In order to obtain more insight into the particle sizes of the Pt and TiO_2 nanoparticles, TEM analysis was performed. The high-resolution TEM (HRTEM) image, EDX mapping and selected area electron diffraction pattern of the 0.6 wt.% Pt-loaded mesoporous-assembled TiO_2 are shown in Fig. 7. The HRTEM image clearly verifies that highly crystalline TiO_2 is formed, due to the presence of apparent lattice fringes. The Pt phase is seen as a dark patch, indicating high electron density, as confirmed by EDX mapping. The particle sizes of the Pt and the TiO_2 from HRTEM analysis are in the range of 5–8 and 10–15 nm, respectively. The observed particle size of TiO_2 is in good accordance with the crystallite size calculated from the XRD result (13.64 nm), signifying that each grain can be considered to be a single crystal. From the SAED pattern presented in the inset of the HRTEM image, all of the electron diffraction rings can be indexed to the anatase phase of TiO_2, which also agrees well with XRD analysis. As a result of N_2 adsorption–desorption, SEM, and TEM analyses, the mesoporous structure of the synthesized TiO_2 nanocrystal can plausibly originate from the pores formed between the nanocrystalline TiO_2 particles in their aggregated assembly.

3.2. Photocatalytic activity for hydrogen production

3.2.1. Effect of photocatalyst type

For each experiment, 0.2 g of a given TiO_2 photocatalyst was first suspended in 150 cm^3 of a 15 vol.% DEA aqueous solution without and with dissolved 0.1 mM E.Y. at room temperature. The photocatalytic activities of different mesoporous-assembled

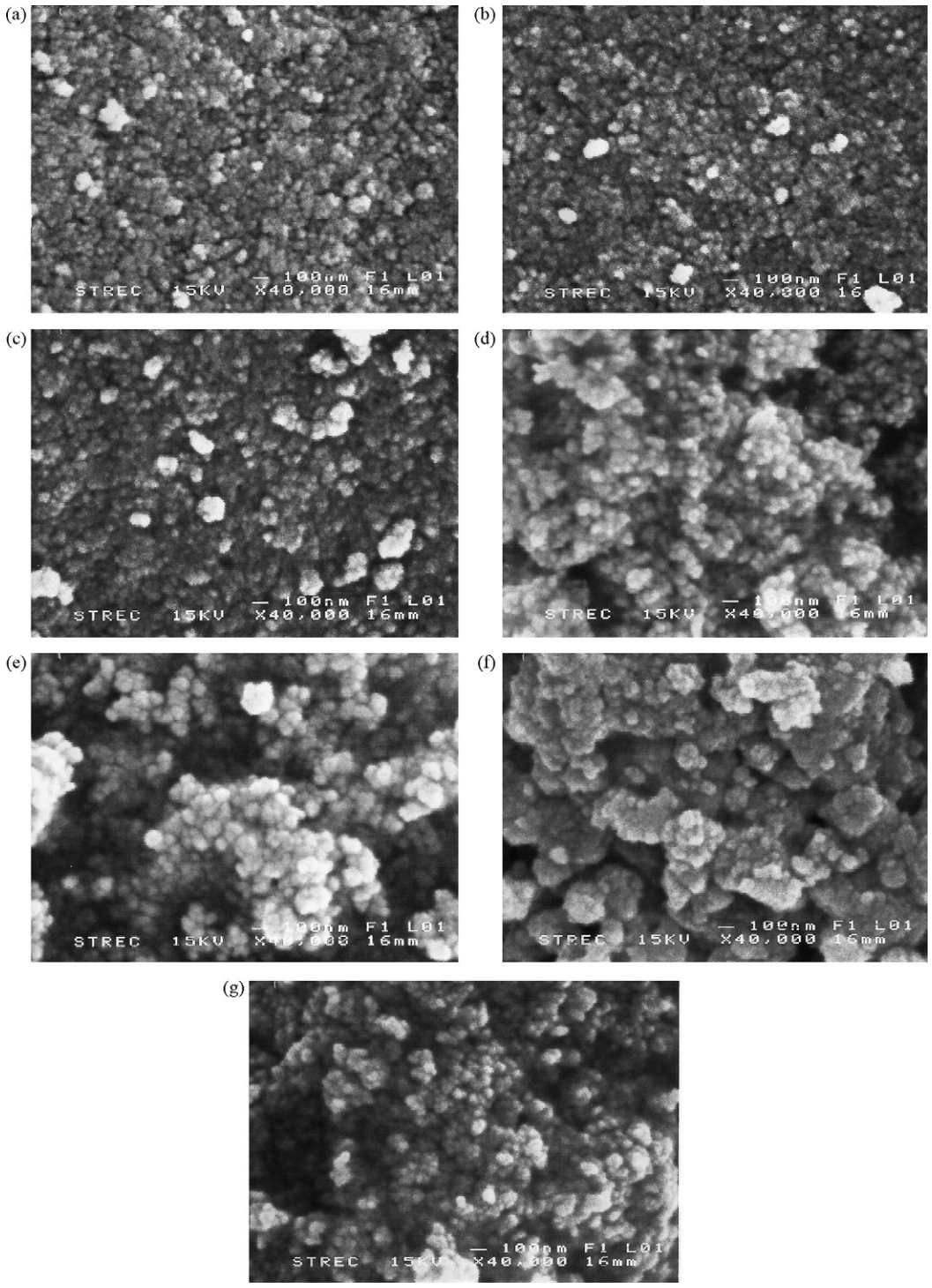

Fig. 5. SEM images of: (a) synthesized TiO_2 calcined at 500 °C; (b) synthesized TiO_2 calcined at 600 °C; (c) synthesized TiO_2 calcined at 700 °C; (d) P-25 TiO_2; (e) ST-01 TiO_2; (f) JRC-01 TiO_2; (g) JRC-03 TiO_2.

TiO_2 samples calcined at 500, 600 and 700 °C (named as TiO_2 500 °C, TiO_2 600 °C and TiO_2 700 °C, respectively) and the 0.6 wt.% Pt-loaded mesoporous-assembled TiO_2 sample calcined at 500 °C (named as Pt/TiO_2 500 °C) in both E.Y.-free and E.Y.-containing systems were compared with the commercial TiO_2 photocatalysts in an E.Y.-containing system under identical reaction conditions. It should be noted that there is no detectable hydrogen production in the absence of visible light irradiation, undoubtedly indicating its importance for the photocatalytic system.

The hydrogen production rates on the various investigated photocatalysts are shown in Figs. 8 and 9. The E.Y.-containing systems provide higher photocatalytic activity for hydrogen production than the E.Y.-free systems, indicating that the E.Y. sensitizer is greatly involved in enhancing photocatalytic hydrogen production. This can be explained by the adsorption of the E.Y. sensitizer on to the photocatalyst surface serving as a mediated path for electron transport from the excited sensitizer to the surface of the photocatalyst, resulting in a sufficiently higher amount of electrons becoming available for water reduction to produce hydrogen. In Fig. 8, it can

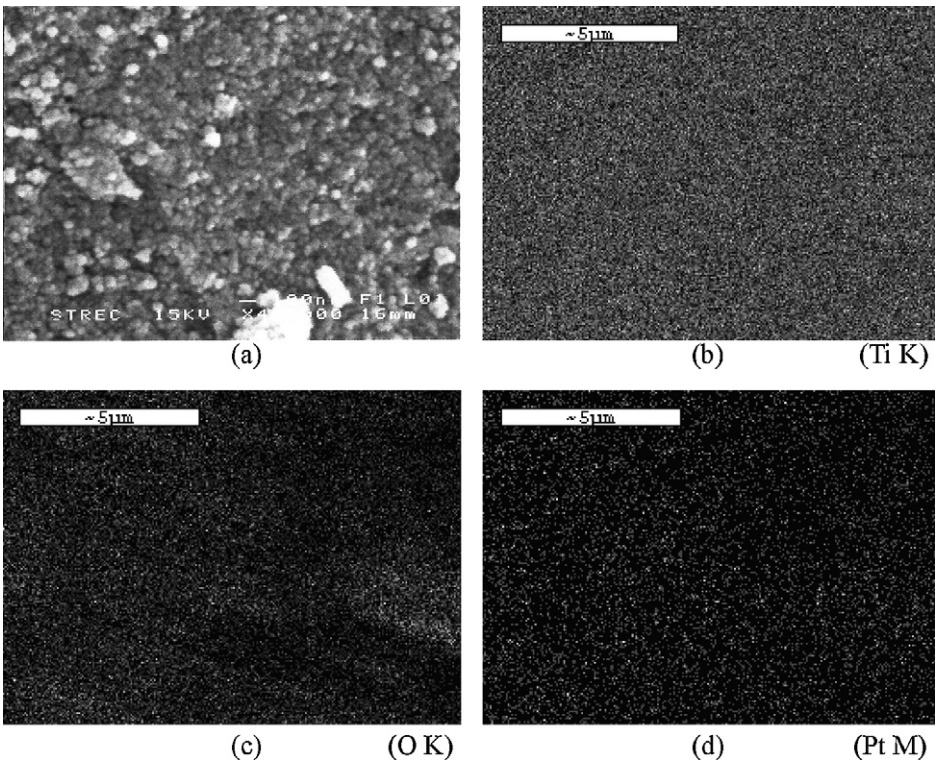

Fig. 6. (a) SEM image of 0.6 wt.% Pt-loaded mesoporous-assembled TiO_2 calcined at 500 °C and EDX elemental area mappings: (b) Ti; (c) O; (d) Pt.

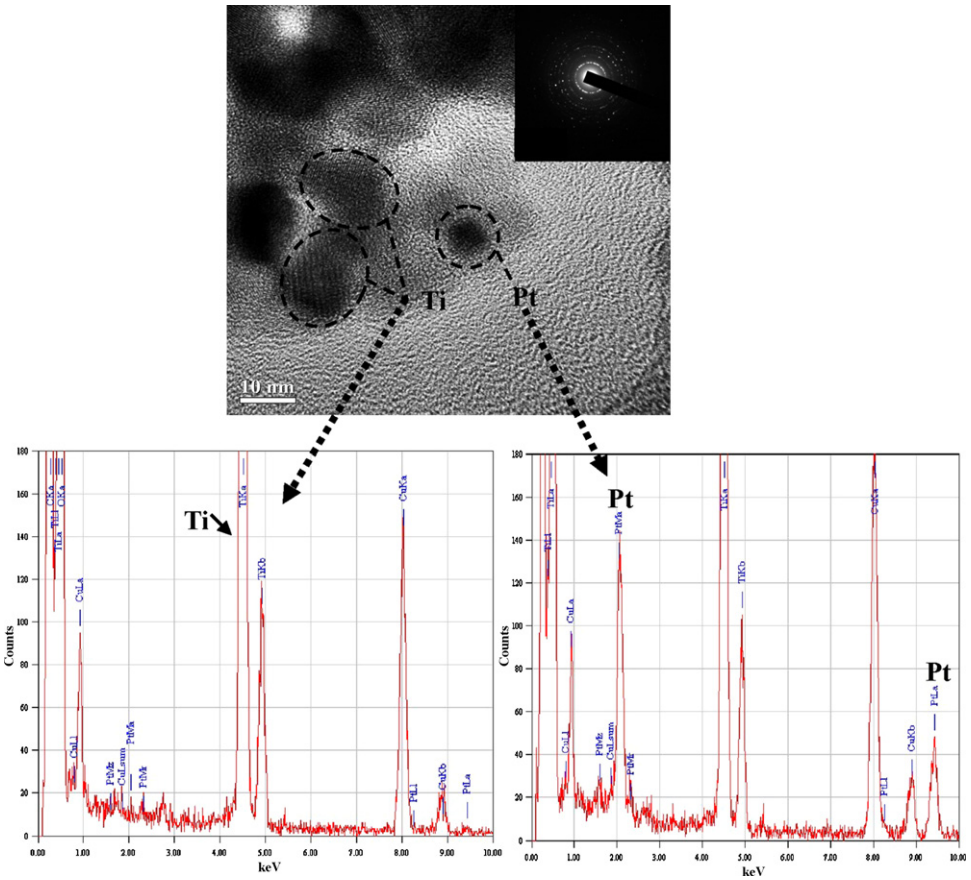

Fig. 7. High-resolution TEM (HRTEM) image and EDX elemental point mappings of 0.6 wt.% Pt-loaded TiO_2 calcined at 500 °C (inset of HRTEM image: selected-area electron diffraction (SAED)).

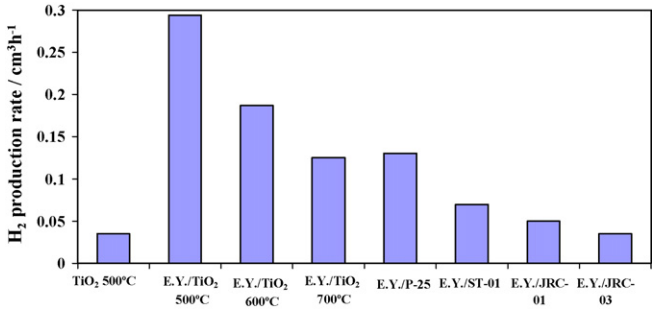

Fig. 8. Effect of photocatalyst type on hydrogen production activity of mesoporous-assembled TiO_2 photocatalyst calcined at different temperatures for 4 h in both E.Y.-free and E.Y.-containing systems compared with commercial TiO_2 photocatalysts in E.Y.-containing system (photocatalyst, 0.2 g; total volume, 150 cm^3 comprising 22.5 cm^3 DEA and 127.5 cm^3 distilled water; E.Y. concentration, 0.1 mM; initial solution pH, 11; reaction time, 4 h).

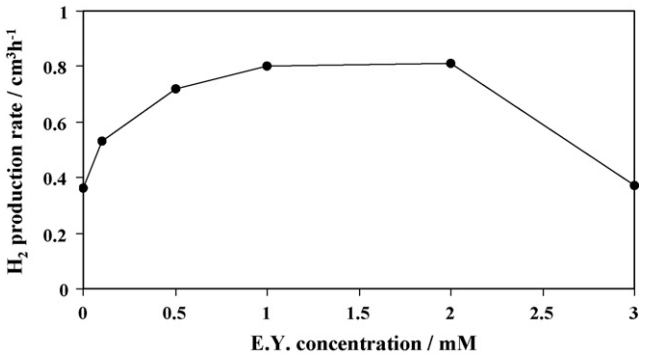

Fig. 10. Effect of E.Y. concentration on hydrogen production activity of 0.6 wt.% Pt-loaded mesoporous-assembled TiO_2 calcined at 500 °C for 4 h (photocatalyst, 0.2 g; total volume, 150 cm^3 comprising 22.5 cm^3 DEA and 127.5 cm^3 distilled water; initial solution pH, 11; reaction time, 4 h).

be seen that the rate of hydrogen production of the mesoporous-assembled TiO_2 calcined at 500 °C from the E.Y.-containing system is much higher than that of the mesoporous-assembled TiO_2 calcined at 500 °C from the E.Y.-free system and all of the commercial TiO_2 photocatalysts from the E.Y.-containing system. Despite the large surface area of about 289.5 $m^2\,g^{-1}$ of the ST-01 TiO_2, the imperfect crystallization (from the XRD data, Fig. 2) and the non-uniform and large pore size distribution (inset of Fig. 1(d)) are believed to increase the probability of mutual electron-excited sensitizer recombination at the surface defects of the photocatalyst. In the case of the P-25 TiO_2, the phase combination between the anatase and the rutile phases (rutile ratio of 0.26, as shown in Table 2) may be the cause of the very low photocatalytic activity. It can be deduced that the presence of a greater amount of the rutile phase exerts a negative effect on the photocatalytic activity, as previously reported in several articles [9,31,32]. By considering the location of the conduction band level, the decrement in the photocatalytic activity can be attributed to the lower flat band potential of the rutile phase that exists at almost a similar level to the SHE potential (H^+/H_2 level), whereas that of the anatase phase is shifted negatively by approximately 0.2 eV [33]. As a consequence, in the case of the anatase TiO_2, the driving force for water reduction is satisfactorily high, while the driving force in the case of the rutile TiO_2 is lower. Moreover, the lack of a mesoporous-assembled structure in the commercial TiO_2 powders (P-25 TiO_2, ST-01 TiO_2, JRC-01 TiO_2 and JRC-03 TiO_2) may lead to less reactant accessibility to the photocatalyst surface for the photocatalytic reaction. By contrast, the use of a nanocrystalline mesoporous-assembled TiO_2 with uniform pore size could decrease the number of lattice defects and then facilitate electron transport for reaction with water molecules adsorbed at the TiO_2 surface along the mesoporous-assembled structure [24].

Apart from the significance of the use of the E.Y. sensitizer and the existence of the mesoporous structure in enhancing the photocatalytic activity, Pt loading is also experimentally found to have a pronounced effect on the photosensitized rate of hydrogen production (Fig. 9). When the mesoporous-assembled TiO_2 photocatalyst without Pt loading is used for the photocatalytic reaction, the hydrogen production rate is only 0.29 $cm^3\,h^{-1}$. For the synthesized mesoporous-assembled TiO_2 with 0.6 wt.% Pt loading, however, the hydrogen production rate is increased markedly to 0.47 and 0.53 $cm^3\,h^{-1}$ for systems without and with E.Y., respectively. This can be explained by the loaded Pt nanoparticles enhancing both sensitizer adsorption and charge separation between the electrons and the excited sensitizer [14]. In this work, other metals (namely Ag, Ni and Cu) at 1.5 wt.% loading have also been deposited on the mesoporous-assembled TiO_2 by the SSSG process [34,35] and used for a comparative hydrogen production study. It is found (Fig. 10) that Pt-loaded TiO_2 exhibits superior performance in enhancing the sensitized photocatalytic hydrogen production activity over the Ag-loaded TiO_2, whereas both the Ni- and the Cu-loaded TiO_2 revealed a negative effect, with much lower photocatalytic activity than the unloaded TiO_2. These results attest to the excellent properties of Pt loaded on TiO_2 for the photocatalytic water splitting reaction, as reported in many other articles [25,36–41].

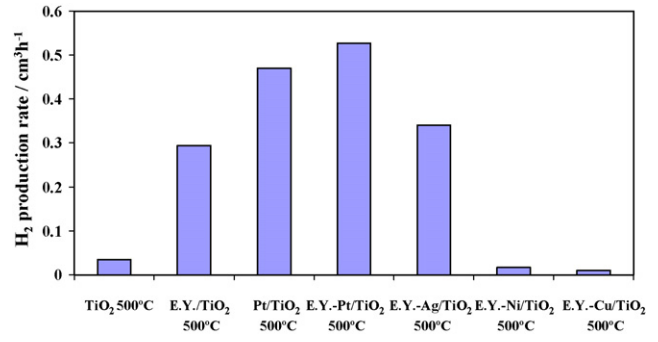

Fig. 9. Effect of metal loading on hydrogen production activity of mesoporous-assembled TiO_2 calcined at 500 °C in both E.Y.-free and E.Y.-containing systems (photocatalyst, 0.2 g; total volume, 150 cm^3 comprising 22.5 cm^3 DEA and 127.5 cm^3 distilled water; Pt, Ag, Ni and Cu loading at 0.6, 1.5, 1.5 and 1.5 wt.%, respectively; E.Y. concentration, 0.1 mM; initial solution pH, 11; reaction time, 4 h).

3.2.2. *Effect of E.Y. concentration*

The concentration of E.Y. plays a significant role in the number of electrons transported from the excited E.Y. to the TiO_2 conduction band, resulting in enhancement of the photocatalytic hydrogen production activity. As noted above, the 0.6 wt.% Pt-loaded mesoporous-assembled TiO_2 exhibits the highest activity for photocatalytic hydrogen production. Therefore, it has been further used as the photocatalyst to investigate the effect of E.Y. concentration on the sensitized photocatalytic activity. The effect of dissolved E.Y. concentration on photocatalytic hydrogen production is shown in Fig. 10. It is found that the hydrogen production rate increases with increasing E.Y. concentration and reaches a maximum at 2 mM (hydrogen production rate of 0.81 $cm^3\,h^{-1}$). With further increase in E.Y. concentration beyond 2 mM, the hydrogen production rate significantly decreases. To explain this behaviour, it is thought that only the fraction of the E.Y. sensitizer adsorbing on the photocatalyst surface is photocatalytically active, directly leading to electron injection into the photocatalyst conduction band [42]. Initially, this fraction increases with increasing E.Y. concentration; hence, the hydrogen production rate increases significantly. If

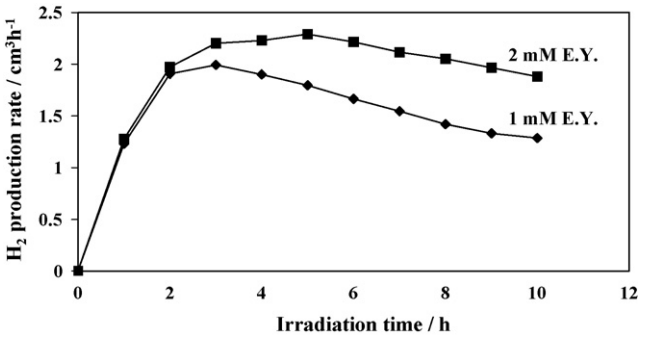

Fig. 11. Comparison of photocatalytic activity using an E.Y. concentration of 1 and 2 mM for 0.6 wt.% Pt-loaded mesoporous-assembled TiO_2 calcined at 500 °C for 4 h (photocatalyst, 0.2 g; total volume, 150 cm^3 comprising 22.5 cm^3 DEA and 127.5 cm^3 distilled water; initial solution pH at E.Y. concentration of 1 and 2 mM, 11.2 and 11.5, respectively; reaction time, 10 h).

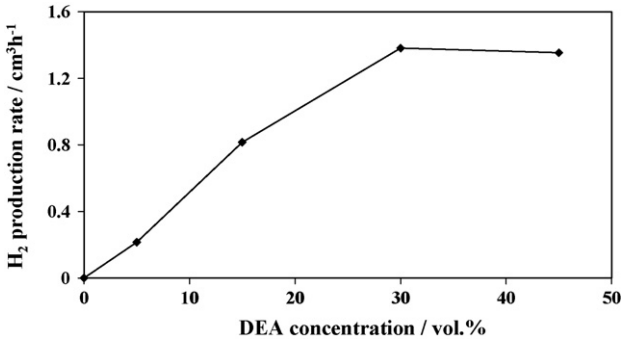

Fig. 12. Effect of DEA concentration on hydrogen production activity of 0.6 wt.% Pt-loaded mesoporous-assembled TiO_2 calcined at 500 °C for 4 h (photocatalyst, 0.2 g; total volume, 150 cm^3 comprising DEA and distilled water; E.Y. concentration, 2 mM; initial solution pH, 11.0–11.6; reaction time, 4 h).

all the photocatalytically active sites are entirely adsorbed by the E.Y. sensitizer, there would be no further increase in the hydrogen production rate with further increase in the E.Y. concentration due to saturation of the E.Y. adsorption sites. Thus, with further increasing E.Y. concentration beyond the optimum value (2 mM), the amount of adsorbed E.Y. does not increase. This, however, undesirably causes an increase in light absorption by the free E.Y. in the bulk solution [21]. Therefore, the number of photons absorbed by the E.Y. adsorbed on the surface of the 0.6 wt.% Pt/TiO_2 photocatalyst is reduced due to the light screening effect of this free E.Y. and results in a marked decrease in the rate of hydrogen production. Furthermore, when the E.Y. concentration is higher than the optimum value (2 mM), the deactivation of the excited E.Y. can occur much more easily and rapidly due to the intermolecular quenching of the adjacent E.Y. on the photocatalyst surface, leading to an ineffective use of the excited E.Y. [43].

In addition, as clearly seen in Fig. 10, an E.Y. concentration of 1 mM gives a slightly lower photocatalytic activity than that of 2 mM; the hydrogen production rates are 0.80 and 0.81 $cm^3\,h^{-1}$, respectively. In order to verify further the exact optimum E.Y. concentration, stability experiments for photocatalytic hydrogen production over the 0.6 wt.% Pt-loaded mesoporous-assembled TiO_2 with two E.Y. concentrations (1 and 2 mM) were conducted for a longer irradiation time (10 h). As shown in Fig. 11, the photocatalytic activity of the E.Y.–Pt/TiO_2 at an E.Y. concentration of 2 mM is higher than that at 1 mM for long-term irradiation, i.e., the photocatalyst in the 2 mM E.Y.-containing solution has higher stability. The E.Y. concentration of 2 mM was therefore used for further photocatalytic activity tests.

3.2.3. Effect of DEA concentration

In the photosensitized hydrogen production system, the electron donor (DEA in this work) plays an important role in regenerating the electron-deficient sensitizer (oxidized sensitizer) after injecting electrons into the photocatalyst conduction band. In order to obtain higher photosensitized efficiency in converting the absorbed visible light into hydrogen energy, a fast electron injection from the excited sensitizer and a slow backward reaction between the electrons and the oxidized sensitizer are required. The function of DEA in the present photosensitized hydrogen production system could be described by: (i) the DEA could quench the oxidized sensitizer species to the ground state by reacting with the oxidized sensitizer species via the electron donation process, or (ii) it could prolong the stability and lifetime of the sensitizer in the photosensitized system for sustaining long-term hydrogen production [21]. The effect of DEA working as the sensitizer regenerator was examined. The photocatalytic hydrogen production activity of the synthesized 0.6 wt.% Pt-loaded mesoporous-assembled TiO_2 photocatalyst at various DEA concentrations is presented in Fig. 12. The results show that there is no hydrogen production under visible light irradiation from the 2 mM E.Y.-containing system without added DEA, thereby indicating the vital role of DEA in the photocatalytic system. Moreover, the photocatalytic hydrogen production rate increases with increasing DEA concentration, and reaches a maximum at 30 vol.% DEA (hydrogen production rate of about 1.38 $cm^3\,h^{-1}$). Because the optimum DEA concentration levels off, the hydrogen production is not increased with further increase in DEA concentration beyond the optimum value, probably because a DEA concentration of 30 vol.% is sufficient for regenerating or quenching the oxidized sensitizer, as well as preventing electron-excited sensitizer recombination. Therefore, excess DEA in the system is not required. Since the 30 vol.% DEA was experimentally verified to be the most suitable electron donor concentration for the investigated system, it was used as a base condition for further experiments.

3.2.4. Effect of photocatalyst dosage

The effect of dosage of the synthesized 0.6 wt.% Pt-loaded mesoporous-assembled TiO_2 nanocrystal photocatalyst in the 30 vol.% DEA aqueous solution containing 2 mM E.Y. on photocatalytic hydrogen production was next investigated. In this work, the photocatalyst dosage was varied in the range of 0–8 g dm^{-3} by adjusting the amount of the photocatalyst added into the reactor under identical solution conditions. The effect of photocatalyst dosage on hydrogen production rate is shown in Fig. 13. It is found that a photocatalyst dosage of 6 g dm^{-3} provides the maximum hydrogen production. Above and below this dosage, a decrease

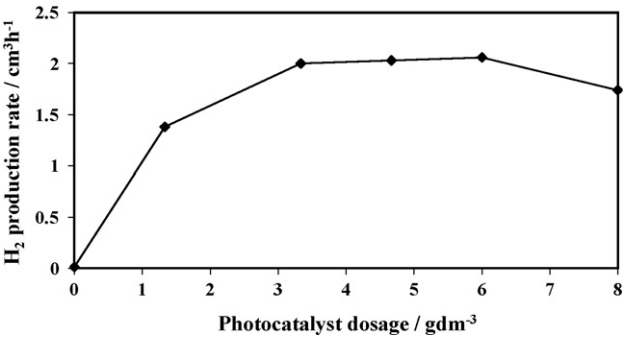

Fig. 13. Effect of photocatalyst dosage on hydrogen production activity of 0.6 wt.% Pt-loaded mesoporous-assembled TiO_2 calcined at 500 °C for 4 h (total volume, 150 cm^3 comprising 45 cm^3 DEA and 105 cm^3 distilled water; E.Y. concentration, 2 mM; initial solution pH, 11.5; reaction time, 4 h).

in hydrogen production rate is observed. A higher dosage of the photocatalyst is expected to correspond to a greater absorption of visible light energy, leading to higher photocatalytic hydrogen production activity. However, the photocatalytic activity starts to decrease when the dosage of the photocatalyst exceeds the optimum value. This indicates that the amount of photocatalyst used needs to be optimized. The results can be explained in terms of both active site availability on the photocatalyst surface for hydrogen production, and irradiating light penetration into the reaction suspension [44]. As the photocatalyst dosage is increased, the number of active sites available for photocatalytic reaction also increases, but the light penetration capability of the system and the subsequent photoactivated region of the reaction suspension decrease. The irradiating light cannot efficiently penetrate throughout the reaction volume because of its blockage by the large quantity of the photocatalyst in the aqueous solution, and results in a lowering of the photon intensity available for the reaction. Although the light absorption of the outermost region of the photocatalyst increases, the capability for hydrogen production from the innermost region decreases due to insufficient photoexcitation. The deactivation of active photocatalyst molecules, due to the agglomeration and sedimentation of the photocatalyst particles as well as undesired collisions between active and ground state photocatalyst molecules, and the consequent decrease in photocatalytic activity have also been reported [44] for photocatalyst dosages that are too high. An optimum amount of photocatalyst is consequently required for the system in order to avoid redundant photocatalyst addition, and also to guarantee total irradiating light absorption for efficient photocatalytic hydrogen production. From the results, a photocatalyst dosage of 3.33 g dm^{-3} (hydrogen production rate of about 2 cm^3 h^{-1}) is considered for further experiments instead of the 6 g dm^{-3} (hydrogen production rate of about 2.06 cm^3 h^{-1}) because the photocatalytic activity is only slightly different; the cost-effectiveness of the Pt source used for synthesizing the Pt-loaded photocatalyst at the lower photocatalyst dosage is also a concern.

3.2.5. Effect of initial solution pH

One of the key parameters affecting photosensitized hydrogen production is the solution pH. The effect of initial solution pH on photocatalytic hydrogen production was studied in the pH range of 8.5–12.5, adjusted by concentrated HCl and NaOH. It should first be noted that the initial pH of the original solution containing 105 cm^3 distilled water and 45 cm^3 DEA is approximately 11.5, and an insignificant change in solution pH is observed during the course of the photocatalytic reaction. Besides, an initial solution pH lower than 8.5 is not possible because there is no further pH decrease upon the addition of concentrated HCl. The effect of the initial solution pH on the hydrogen production rate is shown in Fig. 14. The experimental results indicate that the hydrogen production activity increases with increasing initial solution pH from 8.5 to 11.5, but a further increase in the initial solution pH beyond 11.5 leads to a decrease in hydrogen production. These results imply that the hydrogen production activity of the investigated photosensitized system favours a nearly strong basic solution, and that the optimum initial solution pH is around 11.5. One plausible explanation is that the pH of the solution mainly affects the electron-donating ability of the DEA (or the reducing ability of the lone-pair electrons at the N atom of the DEA).

It has been reported that hydrogen production increases as the initial solution pH is increased, especially at a pH > 6 [45]. This is reasonable because DEA, an amine, can more abruptly donate electrons to the oxidized sensitizer in an alkaline solution since the electron-donating ability of the amine is lower in a more acidic solution because the amine is more protonated [46]. Consequently, the rate of sensitizer regeneration would be enhanced in a more alkaline solution. Therefore, unfavourable back reactions of the excited sensitizer would be inhibited, and the efficiency of the excited sensitizer utilization would be improved. Finally, the hydrogen production rate is greatly enhanced. However, when the initial solution pH is beyond the optimum value (too alkaline), the complexity of coulombic repulsion/interaction among the OH^-, the DEA, the sensitizer and the photocatalyst surface may play a negative role in the reduction of the photocatalytic hydrogen production activity. Since the effect of solution pH is extremely complicated, further experiments are required to obtain a better understanding of the photocatalytic reaction. Detailed results and discussion will be presented in future work.

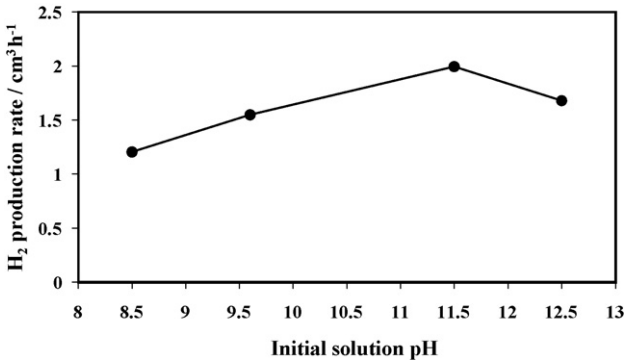

Fig. 14. Effect of initial solution pH on hydrogen production activity of 0.6 wt.% Pt-loaded mesoporous-assembled TiO_2 calcined at 500 °C for 4 h (photocatalyst, 0.5 g; total volume, 150 cm^3 comprising 45 cm^3 DEA and 105 cm^3 distilled water; E.Y. concentration, 2 mM; reaction time, 4 h).

4. Conclusions

Various types of TiO_2 photocatalyst, namely synthesized mesoporous-assembled TiO_2 without and with Pt loading and commercial non-mesoporous-assembled TiO_2 (P-25 TiO_2, ST-01 TiO_2, JRC-01 TiO_2 and JRC-03 TiO_2), have been comparatively studied for sensitized photocatalytic H_2 production under visible light irradiation. The mesoporous-assembled TiO_2 photocatalyst was synthesized by a sol–gel process with the aid of a structure-directing surfactant, whereas the Pt-loaded mesoporous-assembled TiO_2 was synthesized by a single-step sol–gel process.

To improve the visible light utilization of the synthesized TiO_2, the addition of E.Y. as a sensitizer to the photocatalytic reaction system has been investigated together with the Pt loading on the photocatalyst surface. From the UV–vis spectra results, the E.Y. sensitizer is found to absorb primarily the visible light, which strongly suggests that the sensitizer can be activated by visible light for the sensitized photocatalytic hydrogen production system. Moreover, a well-balanced combination between the E.Y. sensitizer and the DEA electron donor can enhance the photosensitized production of hydrogen. The experimental results reveal that the 0.6 wt.% Pt-loaded mesoporous-assembled TiO_2 calcined at 500 °C exhibits the highest photocatalytic performance for hydrogen production from a 150 cm^3 aqueous 30 vol.% DEA aqueous solution containing dissolved 2 mM E.Y. with a photocatalyst dosage of 3.33 g dm^{-3} and an initial solution pH of 11.5 as the optimum conditions.

Acknowledgments

This work was financially supported by the grants obtained from the Thailand Research Fund (TRF) and the Commission on Higher Education, Thailand, and from Chulalongkorn University, Thailand, through the Grants for Development of New Faculty

Staff under the Ratchadapisek Somphot Endowment Fund. The partial support from the Sustainable Petroleum and Petrochemicals Research Unit, Center for Petroleum, Petrochemicals, and Advanced Materials, Chulalongkorn University, Thailand, and from the Petrochemical and Environmental Catalysis Research Unit under the Ratchadapisek Somphot Endowment Fund, Chulalongkorn University, Thailand, is also greatly acknowledged. The authors are also grateful to Prof. Susumu Yoshikawa, Institute of Advanced Energy, Kyoto University, Japan, for invaluable advice.

References

[1] D.J. Wuebbles, A.K. Jain, Fuel Process. Technol. 71 (2001) 99–119.
[2] M.A. Pena, J.P. Gomez, J.L.G. Fierro, Appl. Catal., A: Gen. 144 (1996) 7–57.
[3] J.N. Armor, Appl. Catal., A: Gen. 176 (1999) 159–176.
[4] A. Steinfeld, Sol. Energy 78 (2005) 603–615.
[5] M. Assokkumar, Int. J. Hydrogen Energy 23 (1998) 427–438.
[6] R.C. Saxena, D. Seal, S. Kumar, H.B. Goyal, Renew. Sust. Energy Rev. 12 (2008) 1909–1927.
[7] A.J. Bard, M.A. Fox, Acc. Chem. Res. 28 (1995) 141–145.
[8] M. Matsuoka, M. Kitano, M. Takeuchi, K. Tsujimaru, M. Anpo, J.M. Thomas, Catal. Today 122 (2007) 51–60.
[9] M.R. Hoffmann, S.T. Martin, W. Choi, D.W. Bahnemann, Chem. Rev. 95 (1995) 69–96.
[10] A.L. Linsebigler, G. Lu, J.T. Yater Jr., Chem. Rev. 95 (1995) 735–758.
[11] O. Carp, C.L. Huisman, A. Reller, Prog. Solid State Chem. 32 (2004) 33–177.
[12] M. Ni, M.K.H. Leung, D.Y.C. Leung, K. Sumathy, Renew. Sust. Energy Rev. 11 (2007) 401–425.
[13] K. Gurunathan, J. Mol. Catal. A: Chem. 156 (2000) 59–67.
[14] Z. Jin, X. Zhang, G. Lu, S. Li, J. Mol. Catal. A: Chem. 259 (2006) 275–280.
[15] J. Sabate, S. Cervera-March, R. Simarro, J. Gimenez, Int. J. Hydrogen Energy 15 (1990) 115–124.
[16] R. Abe, K. Hara, K. Sayama, K. Domen, H. Arakawa, J. Photochem. Photobiol., A: Chem. 137 (2000) 63–69.
[17] K.B. Dhanalakshmi, S. Latha, S. Anandan, P. Maruthamuthu, Int. J. Hydrogen Energy 26 (2001) 669–674.
[18] R. Abe, K. Sayama, Chem. Phys. Lett. 362 (2002) 441–444.
[19] R. Abe, K. Hara, K. Sayama, H. Arakawa, J. Photochem. Photobiol., A: Chem. 166 (2004) 115–122.
[20] Q. Li, G. Lu, J. Mol. Catal. A: Chem. 266 (2007) 75–79.
[21] X. Zhang, Z. Jin, Y. Li, S. Li, G. Lu, J. Power Sources 166 (2007) 74–79.
[22] Y. Li, C. Xie, S. Peng, G. Lu, S. Li, J. Mol. Catal. A: Chem. 282 (2008) 117–123.
[23] X. Zhang, Z. Jin, Y. Li, S. Li, G. Lu, Appl. Surf. Sci. 254 (2008) 4452–4456.
[24] T. Sreethawong, Y. Suzuki, S. Yoshikawa, J. Solid State Chem. 178 (2005) 329–338.
[25] T. Sreethawong, S. Yoshikawa, Int. J. Hydrogen Energy 31 (2006) 786–796.
[26] F. Rouquerol, J. Rouquerol, K. Sing, Adsorption by Powders and Porous Solids: Principles, Methodology and Applications, Academic Press, San Diego, 1999.
[27] L. Lin, W. Lin, J.L. Xie, Y.X. Zhu, B.Y. Zhao, Y.C. Xie, Appl. Catal., B: Environ. 75 (2007) 52–58.
[28] B.D. Cullity, Elements of X-ray Diffraction, Addison-Wesley Publication Company, Massachusetts, 1978.
[29] J.V. Smith (Ed.), X-ray Powder Data File, American Society for Testing Materials, 1960.
[30] R.A. Spurr, H. Myers, Anal. Chem. 29 (1957) 760–762.
[31] K.E. Karakitsou, X.E. Verykios, J. Phys. Chem. 97 (1993) 1184–1189.
[32] S. Ichikawa, R. Doi, Thin Solid Films 292 (1997) 130–134.
[33] T. Bak, J. Nowotny, M. Rekas, C.C. Sorrell, Int. J. Hydrogen Energy 27 (2002) 991–1022.
[34] T. Sreethawong, Y. Suzuki, S. Yoshikawa, Int. J. Hydrogen Energy 30 (2005) 1053–1062.
[35] T. Sreethawong, S. Yoshikawa, Catal. Commun. 6 (2005) 661–668.
[36] K. Lee, W.S. Nam, G.Y. Han, Int. J. Hydrogen. Energy 29 (2004) 1343–1347.
[37] T. Sreethawong, T. Puangpetch, S. Chavadej, S. Yoshikawa, J. Power Sources 165 (2007) 861–869.
[38] J.J. Zou, H. He, L. Cui, H.Y. Du, Int. J. Hydrogen Energy 32 (2007) 1762–1770.
[39] Y. Ikuma, H. Bessho, Int. J. Hydrogen Energy 32 (2007) 2689–2692.
[40] H. Yi, T. Peng, D. Ke, D. Ke, L. Zan, C. Yan, Int. J. Hydrogen Energy 33 (2008) 378–672.
[41] M.A. Khan, M.S. r Akhtar, S.I. Woo, O.B. Yang, Catal. Commun. 10 (2008) 1–5.
[42] D. Duonghong, E. Borgarello, M. Gratzel, J. Am. Chem. Soc. 103 (1981) 4685–4690.
[43] J.E. Moser, M. Gratzel, J. Am. Chem. Soc. 106 (1984) 6557–6564.
[44] I.K. Konstantinou, T.A. Albanis, Appl. Catal., B: Environ. 49 (2004) 1–14.
[45] E.A. Malinka, G.L. Kamalov, J. Photochem. Photobiol., A: Chem. 81 (1994) 193–197.
[46] H. Dürr, S. Boßmann, A. Beuerlein, J. Photochem. Photobiol., A: Chem. 73 (1993) 233–245.